Scientific Research Publishing

International Journal of Geosciences, 2025, 16(11), 815-836
https://www.scirp.org/journal/ijg
ISSN Online: 2156-8367
ISSN Print: 2156-8359

# Gravimetric Reconstruction of the Citlaltépetl-Teteltzingo Volcanic Complex at 32 ka

**Román Alvarez[1*], Miguel Camacho-Ascanio[2]**

[1]Applied Mathematics and Systems Research Institute (IIMAS), National Autonomous University of Mexico (UNAM), Mexico City, Mexico
[2]Geophysics Institute, National Autonomous University of Mexico (UNAM), Mexico City, Mexico
Email: *roman.alvarez@iimas.unam.mx

**How to cite this paper:** Alvarez, R. and Camacho-Ascanio, M. (2025) Gravimetric Reconstruction of the Citlaltépetl-Teteltzingo Volcanic Complex at 32 ka. *International Journal of Geosciences*, **16**, 815-836.
https://doi.org/10.4236/ijg.2025.1611040

**Received:** September 30, 2025
**Accepted:** November 8, 2025
**Published:** November 11, 2025



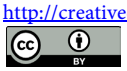



## Abstract

The remaining fault scarps of a collapsed structure at 32 ka, named Tetelzingo crater, that included Citlaltépetl (CT) volcano, and the associated gravity field, are the basis of a reconstruction of the structures involved. The gravity field is obtained from the GGMplus model, from which 3D inversions at resolutions of 1000, 500, and 250 m are performed. Low-gravity anomalies are associated with Sierra Negra (4580 m) and Citlaltépetl (5521 m) volcanoes, as well as with the Chichimeco Dome Complex (~4000 m) (CDC). They are located within a SW-NE anomaly that serves as a constraint to the reconstruction. The associated Bouguer anomaly appears as a continuous low-gravity surface; however, its vertical derivative Dz shows that the sources of those three structures are separated. The fault scarps are complemented with inferred trajectories that suggest the existence of two volcanoes before the collapse at 32 ka: Citlaltépetl and the Ancestral Teteltzingo. Density cross-sections identify three stratified magmatic deposits under the summit of CT. On the summit of CT, there is an anomalous concentration of high-density materials, attributed to the presence of domes and lava flows, which mask the position of the volcano's chimney. The existence of the Ancestral Teteltzingo volcano (ATE) is inferred NE of CT from the associated density distribution; CDC is at the center of the ATE structure and is interpreted as a resurgent activity at <8 ka. Sierra Negra volcano (SN) shows low-density distributions in and around its summit, contradicting the idea that this is an extinct volcano.

## Keywords

Citlaltépetl, Pico de Orizaba, Sierra Negra, GGMplus Gravity Data, Plinian Eruptions, Stratified Magma Chamber

## 1. Introduction

The region of Citlaltépetl volcano has experienced volcanic activity since ~650 ka to date [1]. During this lapse, repeated eruptions occurred, as did collapses and resurgences. Recently, Citlaltépetl volcano (CT) has shown sporadic, fumarolic activity for the last 300 years, but no eruptions occurred in this period [2]. CT had several important eruptions during the late Pleistocene and Holocene [3] [4]. **Figure 1** shows a DEM of the study area with Citlaltépetl as the major structure in the area. The former cone has been destroyed by partial gravitational collapse, producing debris-avalanche deposits [5] [6]. An ancestral version of the CT, named the Tetelzingo volcano [7], collapsed at 32 ka, leaving only fault scarps remaining to date, which in this work are the starting point for a reconstruction of the volcanic distribution at 32 ka.

In **Table 1**, we compiled the evolution in time of volcanic activity in the CT area, from the works of three sources.

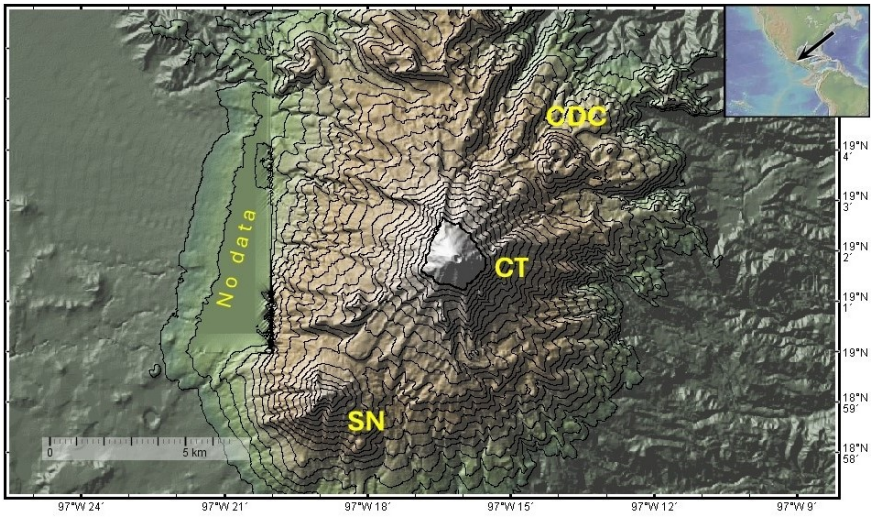


**Figure 1.** Digital Elevation Model (DEM) of Citlaltéptl Volcano (CT) and Sierra Negra (SN) with a contour interval of 200 m between 3000 and 5000 m; a small region to the W contains no data for contouring. CT is the highest volcano in Mexico (5521 m). CDC, Chichimeco Dome Complex. Sierra Negra is a volcanic structure (4580 m) where an important astronomical observatory operates. Map from GeomapApp [8]. A major block-and-ash fan extends over 14 km westward from the summit of CT. Radiocarbon dating of charcoal within the fan deposits yielded Holocene ages that range between 4.0 and 4.6 ka [2].

**Table 1.** Evolution in time of the Citlaltépetl Volcanic complex.

| | Episode | Age (ka) | Manifestation |
|---|---|---|---|
| Copy | Torrecillas, CA | 650 - 290 | Volcano, Collapse at 290 ka |
| | Sierra Negra, CA | 290 | Stratovolcano |
| | Espolón de Oro, CA | 210 - 20 | Volcano, Collapse at 20 ka |
| | Metlac, H&R | 90 - 60 | Volcano |
| | Tecomale, CA | <150 | Dome |
| | Tecomale, R&C | 150 - 80 | Dome |

**Continued**

| | | | |
|---|---|---|---|
| Copy | Tetelzingo, H&R | 80 - 32 | Volcano, Collapse at 32 ka |
| | Chichimeco, H&R | <8.5 | Dome complex |
| | Citlaltépetl, H&R | <10 | Stratovolcano |

Note: CA [1], H&R [7], R&C [3].

Three developing periods for the CT [3]; the first one lasted over a million years, with discontinuous effusive activity. The second one lasted about 100,000 years; they believe that this second period started with the formation of a caldera, ending with the progressive emptying of a surficial, differentiated magma chamber. The most recent phase started at 13 ka and was the most intense event, creating a large crater 4 - 5 km wide in which the present cone grew in this crater. They interpret this eruptive cycle as induced by recurring injections of deep magma within the crustal chamber. They also state that Sierra Negra (SN) has functioned as an advective apparatus of CT. The development of a caldera is doubted since its existence cannot be confirmed, perhaps owing to its cover by subsequent effusions or by erosional dismantlement.

A subsequent study [7] divided activity in the region of CT into three Sequences (I - III) and various Episodes with their corresponding time spans. They place the collapse of the Tetelzingo structure at 33 ka, in Sequence II, Teteltzingo Episode.

## 2. Methods

### 2.1. Data Acquisition

We obtained the high-resolution, satellite-derived gravity data set GGMplus [9] corresponding to the Citlaltépetl volcanic area. It is well known that this data set was acquired within a latitudinal belt that comprises the Earth's region between ±60˚; this belt contains a major oceanic region that is not fully processed. The process for obtaining the Bouguer Anomaly (BA) has been described in various publications, using ground and satellite-derived data [10]-[14]; we refer the reader to those publications for additional details.

Notwithstanding, we can summarize the procedure used here by saying that the raw dataset is obtained from http://ddfe.curtin.edu.au/gravitymodels/GGMplus/; using Gravity Observed ($G_{Obs}$) from it, to calculate the BA according to the new gravimetric standard of the USGS [15]. The elevation at each point must be known; we used the topographic model with a resolution of 15 arc-sec, or ~450 m: https://download.gebco.net/ [16]; see also ETOPO1 [17]. For the topographic correction, we employed the method implemented in the Oasis Montaj program of Geosoft, which uses the algorithm proposed by Kane [18] and supplemented by Nagy [19]. Gravimetry data were prepared for inversion through a Gaussian filter that separates the residual to highlight the structures associated with volcanic edifices. The corresponding map appears in **Figure 2**. Negative gravity anomalies are often related to volcanic edifices associated with the presence of magma chambers and volcanic plumbing systems [10] [11] [13] [20].

## 2.2. The Regional Bouguer Anomaly

Regional gravity anomalies describe the behavior of gravity in extended regions; in the present case, it describes the regional behavior of gravity in a region that is several times the extent of the Pico de Orizaba volcano. The Bouguer Anomaly (BA) map is shown in Figure 2; in the central portion, a major low-gravity region corresponding to Citlaltépetl, the highest volcano in Mexico (5521 m), and accompanying SW, a smaller low-gravity anomaly corresponding to Sierra Negra (SN), where an important astronomical observatory operates. Gravity values in the map display a range of ~200 mGal; the gradient of the BA is observed, with lowest values to the W and highest ones to the E; it is interrupted at the central portion by the CT anomaly. To the W of the anomaly, there is a succession of maxima and minima extending in the N-S direction; in fact, the CT and SN gravity anomalies are located within the easternmost minima of this series.

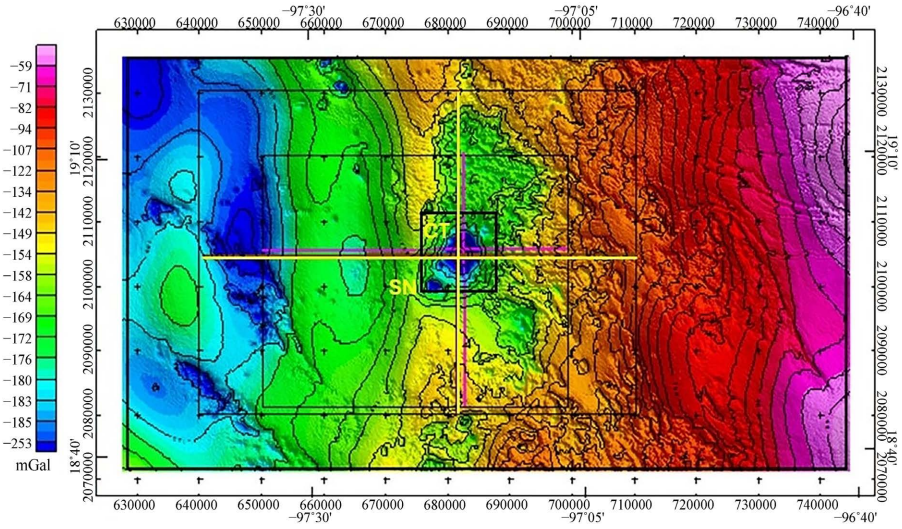


Figure 2. Bouguer Anomaly map of the region containing the CT volcano. Three rectangles (black) show the areas where 3D inversions are performed at 1000, 500, and 250 m resolutions, respectively. SN: Sierra Negra. CT: Citlaltépetl. Yellow and magenta lines show the extent of E-W and N-S density cross-sections obtained from the 3D inversions, all crossing the CT gravity anomaly. Contour lines help visualize the gravity distribution in the area.

## 2.3. Residual Bouguer Anomaly

Figure 3 displays two maps of the residual Bouguer anomaly (BA), one shows the residual BA, and the second includes the DEM of the area superposed to it, showing the correspondence between the topographic elevations and the low values of the residual BA. In this map, in addition to the expected association in the cases of Citlaltépetl volcano (CT) and Sierra Negra (SN), there are two additional, unexpected anomalies, one is located to the N of CT, identified as Cerro Las Cumbres (CLC), and the second is located SE of CT, tentatively named Ixhuatlancillo (IX), NW of Orizaba City. The outstanding negative values, and the clear volcanic origin of CT and CLC make us infer that IX and the two low-gravity locations with question marks are also of magmatic origin.

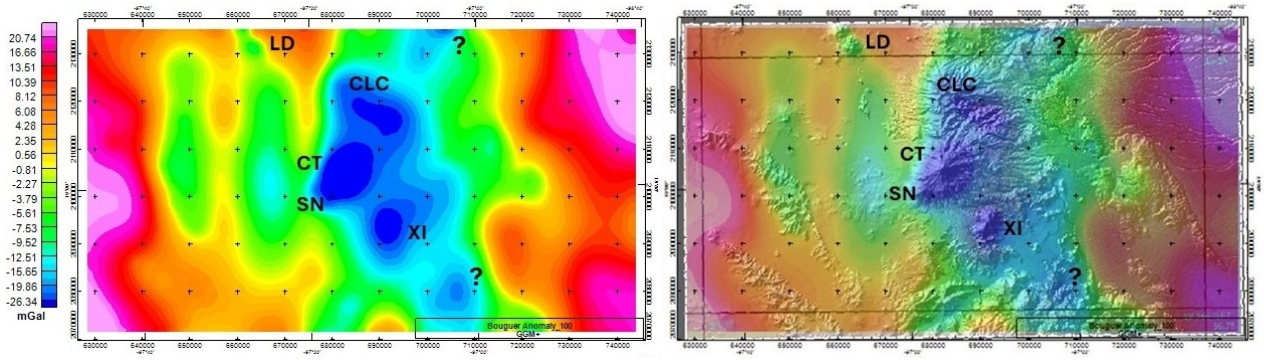


(a) (b)

**Figure 3.** (a) Residual Bouguer anomaly map (GGM plus) showing the regions of low-gravity values associated with several volcanic structures: CT: Citlaltépetl; SN: Sierra Negra; CLC: Cerro Las Cumbres; IX: Ixhuatlancillo Anomaly; LD: Las Derrumbadas. (b) The Bouguer anomaly is superposed on a DEM of the area, showing the correspondence of low-gravity regions with volcanic structures. The two low-gravity locations with question marks may also be of magmatic origin. Notice the smaller interval of gravity values with respect to the Complete Bouguer anomaly in **Figure 2**, creating better anomaly discrimination.

The single, low-gravity anomaly of **Figure 2** has been transformed into three distinct anomalies in **Figure 3**: TL, CT-SN, and IX. Notice that this procedure is not sufficient for separating the Sierra Negra and Citlaltépetl anomalies, since they appear as a single, SW-NE elongated anomaly.

### 2.4. The Vertical Derivative

The derivative of AB in the vertical direction (Dz) helps locate the deeper contributions to the anomaly, as well as to delimit and locate the edges of sources that generate the anomaly. The CT and SN negative anomalies are now separated. The corresponding map appears in **Figure 4**, where we have reproduced the rectangles defining the regions from which 3D inversions were made. The smallest rectangle contains the CT and the SN anomalies, indicating that these anomalies have deep roots. The succession of N-S gravity maxima and minima previously observed in the BA map (**Figure 2**) is enhanced in this Dz map, suggesting that this arrangement could have been induced by an E-W extensional process. We note that two Dz negative anomalies located in the N limit of the map (97˚27'W, 10˚17'N) correspond to Las Derrumbadas rhyolitic domes [21].

## 3. Results

### 3.1. Teteltzingo Crater

Two paths for the remaining fault scarps of the Tetelzingo crater were reported [7], which we reproduce in **Figure 5** as two yellow lines superposed to the SN-CT gravity anomaly. We try to reconstruct the contour of the collapsed region. In **Figure 5**, the two red lines on the extremes of the fault scarps close their trajectories, providing a version of what was interpreted as the single structure that collapsed at 33 ka [7]. The criteria for drawing the red lines that close the fault scarps are, to the NE, the closure must remain within the low-gravity region, whereas to the SW it must include the summit of the present structure.

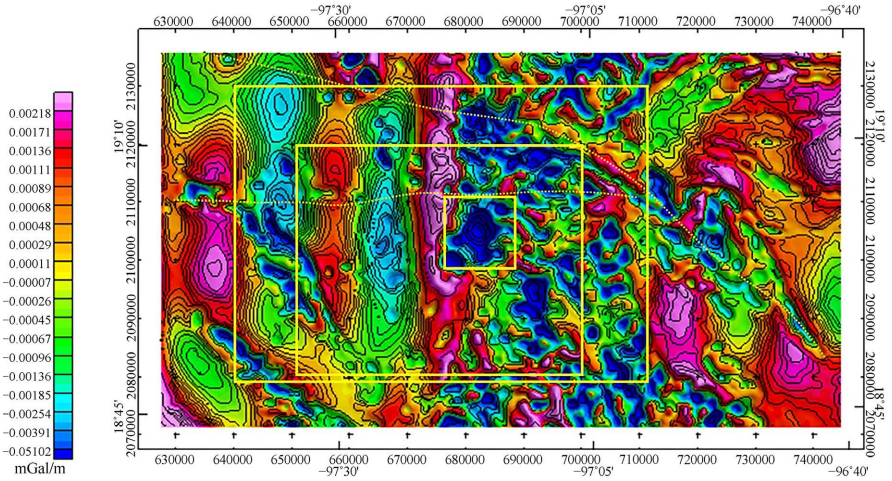


**Figure 4.** First vertical derivative (Dz) of the Bouguer Anomaly, derived from the map in **Figure 2**. The three rectangles in the AB map are reproduced here. From W to E, there is an alternance of vertical, maxima and minima, with a separation between the maxima or minima of ~20 km; the pattern is lost after the presence of the corresponding anomaly of Citlaltépetl (CT). SN: Sierra Negra. The rectangles in **Figure 2** are included for reference. Dashed lines highlight trends that interrupt continuous anomalies.

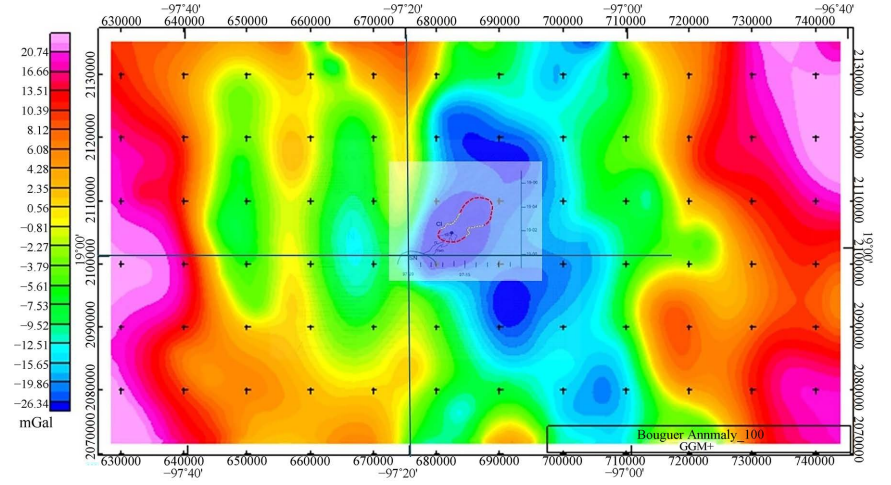


**Figure 5.** Extract of Bouguer anomaly map in **Figure 3**, emphasizing the anomaly region corresponding to Citlaltépetl volcano. A closer look at this reconstruction appears in **Figure 7**. Two yellow lines correspond to the Tetelzingo-crater fault scarps reported [7]. The two red paths connecting the yellow lines are inferred to close the limits of the original ACT crater; all of them fall within the extent of the CT low-gravity anomaly. Outlines are presented of the NE limit of SN, some historic lava fluxes, and the location of the present crater. The color scale is the same as that in **Figure 3**. Reference lines intersect at 97˚20'W, 19˚00'N.

The crater fault scarps get closer at their central parts; to close the perimeter of the collapsed region, in **Figure 5**, we propose two circular paths that close it, outlining what seems to delimit the extent of two volcanic structures at 33 ka. The SW slice belongs to the present location of CT, while the NE portion corresponds to the newly proposed structure to be called Ancestral Tetelzingo (ATE), follow-

ing the nomenclature for other volcanic structures that pre-date the present ones (e.g., Ancestral Popocatépetl, Ancestral Iztaccíhuatl). According to this view, the collapsed region involved two volcanic structures: CT and ATE.

In summary, at 33 ka the collapsed region extended 9 - 10 km in the SW-NE direction. The formation of a crater 4 - 5 km in diameter at 13 ka was reported [7], in which the present cone of CT grew, coinciding in location and size with the SW circle shown in Figure 7.

The configuration in Figure 6 depicts three isolated anomalies (SN, CT, and

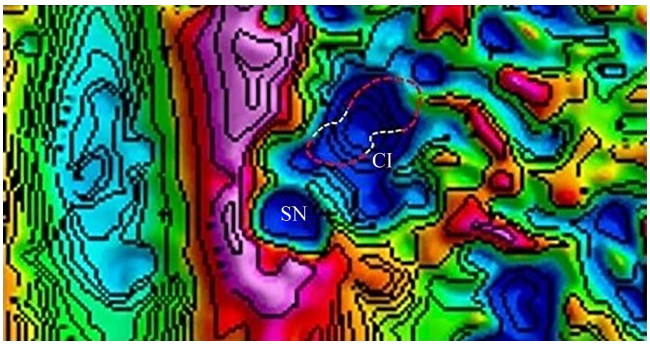


Figure 6. Extract of the vertical derivative (Dz) of the Bouguer anomaly (Figure 4) corresponding to the area of CT with the superposed reconstructed fault scarps. The vertical derivative anomalies for SN, CT, and ATZ appear separated in this map, enhancing the probability of having two independent volcanoes at 33 ka. The contours indicate that the lowest values of the Dz anomaly are associated with the crater region of the present CT; the ATE region coincides with a low of the vertical derivative, separated from CT by a mid-value, circular anomaly (green). CT and SN are also separated by a similar anomaly. The color scale is the same as that in Figure 4.

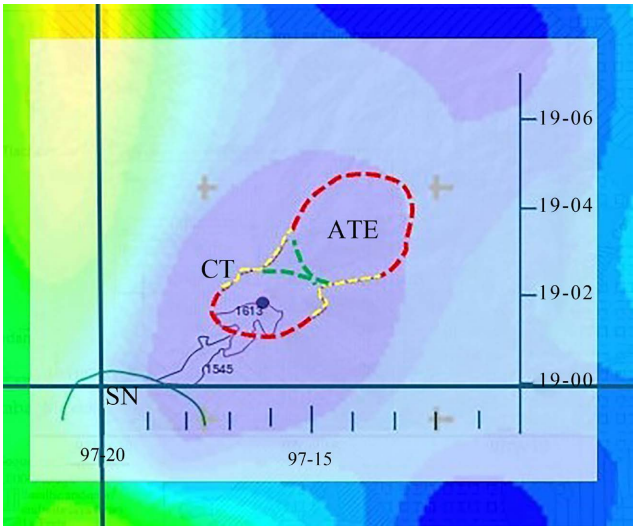


Figure 7. Complementing the reconstruction initiated in Figure 5, two green lines complete two independent circles, suggesting the existence of two coeval volcanic edifices: Citlaltépetl (CT) and Ancestral Teteltzingo (ATE), both located on the low-gravity anomaly corresponding to CT. The black dot represents the present summit caldera of CT. Outlines of historic lava flows that occurred in 1545 and 1613 are indicated. The Sierra Negra (SN) outline shows it at the SW limit of the low-gravity anomaly.

ATE) suggests that the latter two have been independent structures and not the single amphitheater-shaped Tetelzingo crater originally proposed [7]. In **Figure 7**, we complete the reconstruction of the outlines of the two inferred craters: CT and ATE.

The reconstruction proposed in **Figure 7** requires a change in nomenclature since originally it was referred to the Teteltzingo crater as that associated with the fault scarps [7], with an extent of ~9 km as observed in the reconstructions of **Figure 6** and **Figure 7**. The SW structure corresponds to Citlaltépetl; we shall refer to the newly recognized volcanic structure as the Ancestral Tetelzingo (ATE). Judging from the size of the reconstruction circles, we speculate that ATE was probably higher than CT at the time of its collapse at 33 ka. Supporting gravimetric information for this interpretation will be presented ahead, when obtaining cross-sections of the 3D density models from the inversion of the gravity map.

### 3.2. 3D Inversions

The Bouguer anomaly data (mGal) is transformed into density data (g/cm$^3$) using a 3D inversion process; in the present case, three inversions were performed at 1000, 500, and 250 m resolutions. The distribution of the density data is then analyzed and linked to geological materials. The depth of the model is proportional to the resolution, ranging from 15 to 5 km. **Figure 8** shows the 250-m resolution example, illustrating the result of the inversion, showing that depth reaches sea level. In these 3D representations, we often include the corresponding DEM for correlation purposes.

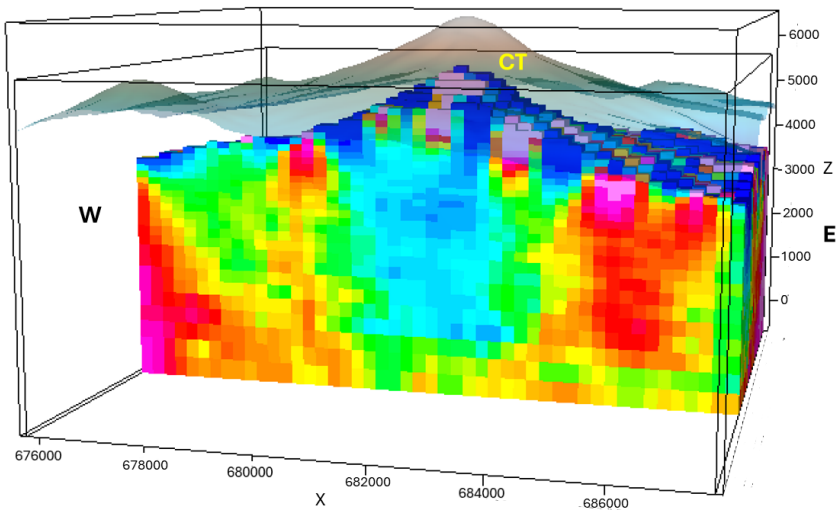


**Figure 8.** An example of the 3D inverted result of the Bouguer Anomaly at 250 m resolution, showing an E-W density cross-section through the summit of the CT Volcano; the model's depth reaches sea level. The DEM is shown on top of the inverted results for correlation purposes. Blue tones correspond to low-density regions, while red tones correspond to higher densities.

### 3.3. Gravity Analyses of the Teteltzingo Area

All of the above observations are of a geologic nature. We shall now present some

geophysical studies based on gravity observations that will complement the geologic ones, particularly since they will describe density distributions from the surface to a given depth. The depth reached by the model depends on its resolution, understood as the size of the unit volume of the model. To exemplify, we consider the 1000-m resolution model, as one that has the same density in a $1 \times 1 \times 1$ km$^3$ volume. As the resolution increases (e.g., $250 \times 250 \times 250$ m), the model tends to better describe the actual density conditions. As the resolution increases, computer time also increases, and a compromise must be made. Another aspect is of importance, as the resolution decreases, the depth of the model increases; the modeler must settle between those parameters, depending on the objective.

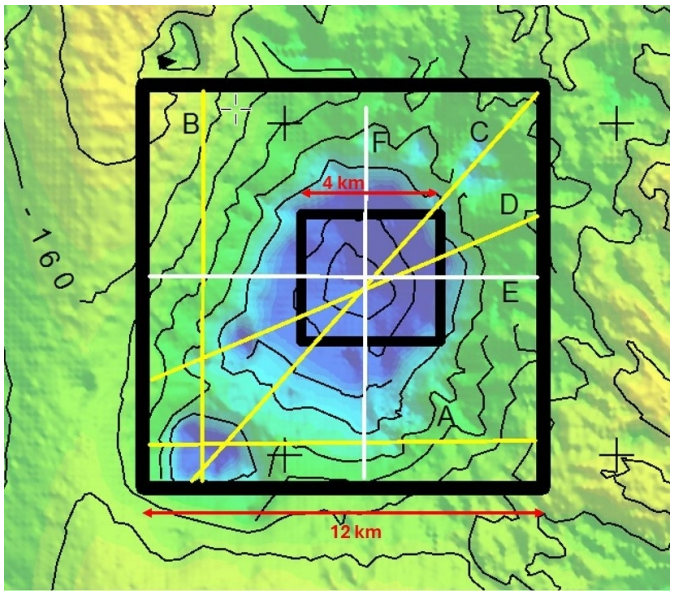


**Figure 9.** Area extracted from the BA map (**Figure 4**). The two rectangles show the areas where 3D inversions were made; the outer rectangle has a resolution of 500 m, whilst the inner one has a resolution of 250 m. Lines are labeled A through F. Lines A, B, and C sample Sierra Negra (SN) on the SW corner, the rest traverse the Citlaltépetl (CT) structure.

### 3.3.1. Cross-Sections at 1000-m Resolution

From the inverted volume at 1000-m resolution, we extracted W-E and N-S cross-sections. **Figure 10(a)** shows the vertical, W-E density cross-section, with an extension of nearly 65 km and a depth from the summit of ~15 km. CT Volcano projects to almost 5000 m altitude because of the size of model's prisms. In connection with **Figure 4**, we located a succession of maxima and minima of Dz; this cross-section confirms this periodicity as a succession of high and low-density regions that extend vertically to the full height of the cross-section. We associate this density arrangement with an E-W extensional process in the region, like the extensional progression associated with the Sierra Nevada [22]. A dashed line indicates a possible trajectory for the feeding of magmatic material to a magmatic deposit close to the summit of the volcano; we locate this deposit at an elevation of +1500 m. In this model, the volcanic chimney is inferred from +2000 m to the summit.

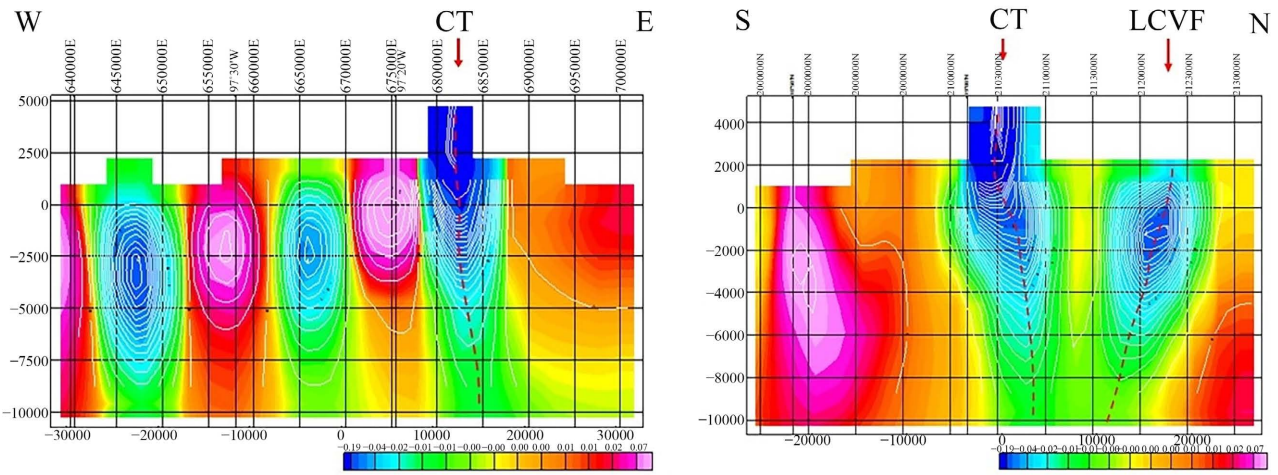


**Figure 10.** (a) Density cross-section, (60 km long, 15 km depth) with a resolution of 1000 m along the horizontal brown line in the map of **Figure 2** (larger rectangle). The observation about the periodicity of high- and low-density regions observed in the Dz map (**Figure 4**) W of CT, is confirmed here. CT is in the easternmost of these elements; the cross-section reaches 15 km in depth, from the summit of the volcano. A red, dashed line indicates a possible path for the recharge, starting at +1000 m of a surficial magmatic deposit. (b) Density cross-section with a resolution of 1000 m, along the vertical (N-S) brown line in the map of **Figure 2** (larger rectangle). It also shows the superficial magma deposit observed in the W-E cross-section, fed from below −10 km depth (red, dashed line); the present volcanic chimney is well-defined by the contour lines. To the N, there is another, deeper magmatic deposit centered at −1000 m depth, in which a low-density channel on the surface might be associated with an ejecta outlet of the Las Cumbres Volcanic Field (LCVF) [7] [23] [24]. The color scales represent density values +2.67 g/cm$^3$.

The N-S cross-section appears in **Figure 10(b)**; the density distribution along this line differs from the distribution in **Figure 10(a)**; here, a low-density anomaly extends from the CT volcano to the N, which constitutes an unexpected result. Two dashed lines indicate potential trajectories for the flux of low-density magmatic materials; one goes to the uppermost magmatic deposit of CT, and the second deviates N, with a center located at −1000 m; this region extends to the surface through a small section of low-density material that resembles an ejecta outlet.

### 3.3.2. Cross-Sections at 500-m Resolution

The E-W density cross-section, at double the resolution of that in **Figure 10(a)** (500 m), appears in **Figure 11**, where the model's depth has been reduced to 6 km. The higher resolution of this model exposes new details of this cross-section. The low-density anomaly associated with CT shows a vertical, elongated minimum located at elevations between +1000 and +2000 m, directly under the volcano's summit, although the depth of the full, low-density region reaches −6000 m. To the W of CT appears the succession of high- and low-density regions found in **Figure 10(a)**. The Sierra Negra-Cofre de Perote volcanic system lies on a zone of normal extensional faults, which are also oriented in an N-S direction and separate the Altiplano highlands from the plains of the Gulf of Mexico [25]. However, such a hypothesis had not been proven at the time of their study [2]. We infer that the density alternation in **Figure 10(a)** and **Figure 11**, west of CT, is induced by an extensional process in the E-W direction, like that reported regarding the Sierra Nevada [22], support-

ing the statement of the former authors.

The N-S density cross-section appears in Figure 12; the density minimum is located under the summit of CT, as in the E-W cross-section (Figure 11). The

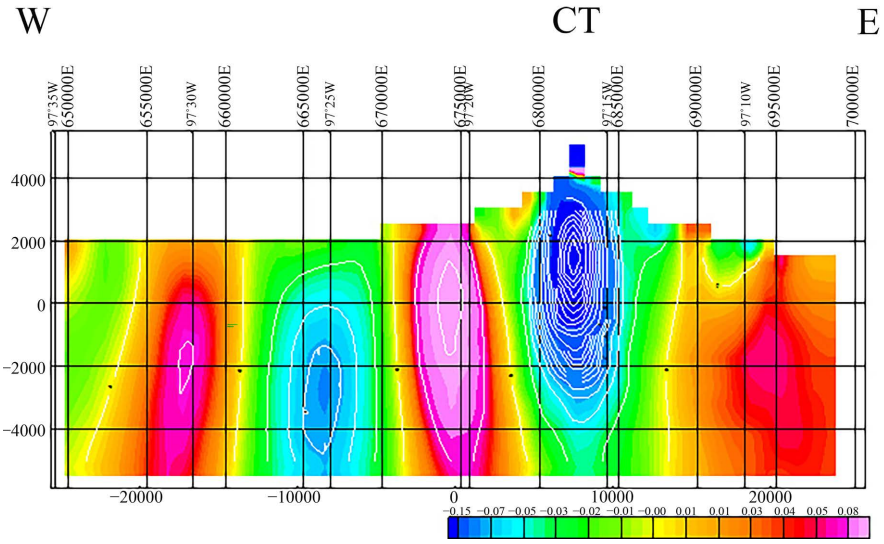


Figure 11. Density cross-section along the horizontal yellow line in the map of Figure 2 (mid rectangle). The extent is nearly 50 km, and the resolution is increased to 500 m; the model reaches a depth of –6 km. The topographic profile of the volcano is more realistic, and the details of the magmatic deposit show better resolution. The color scale represents density values +2.67 g/cm$^3$.

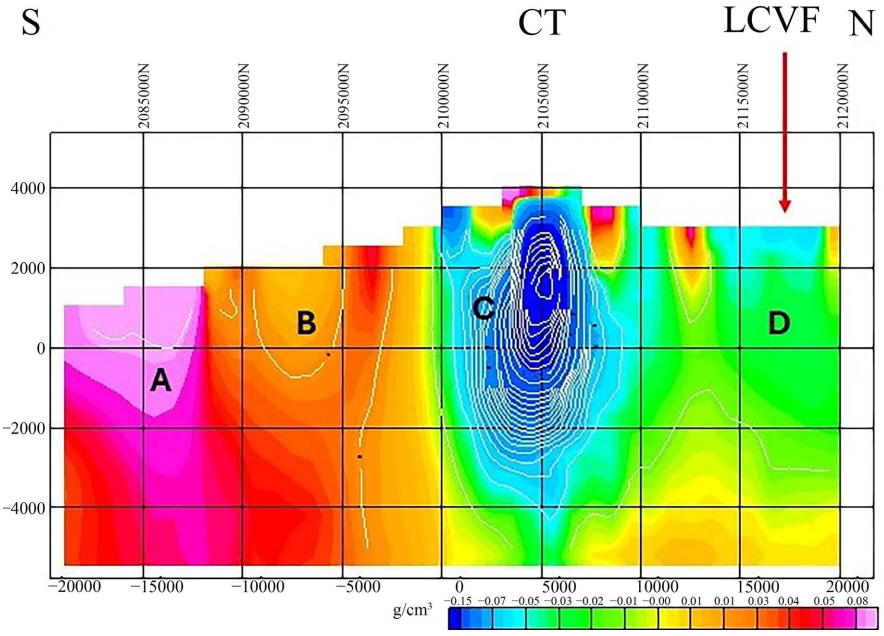


Figure 12. Density cross-section along the vertical (N-S) magenta line in the map of Figure 2 (middle rectangle), the resolution is 500 m. The central portion of the low-density anomaly also appears at +1500 masl. 15 km to the N shows the low-density region described in Figure 10(b), corresponding to Las Cumbres Volcanic Field (LCVF). Regions A-D described in the text. The color scale represents density values +2.67g/cm$^3$.

associated low-density anomaly is wider along this cross-section. A high-density region flanks CT to the S, and to the N appears a mid-density region corresponding to the low-density anomaly (LCVF) located 15 km N of CT (Figure 10(b)). The cross-section now shows a high-density portion (A) 20 km S of the summit, followed to the N by a region (B) of lower density. The summit shows high-and low-density regions (C), followed by a mid-density region (D) corresponding to LCVF. In this projection and at this resolution, a high-density region appears at the summit; we will discuss this region in detail when analyzing the 250-m resolution cross-section.

### 3.3.3. Cross-Sections at 250-m Resolution

At this resolution, the internal configuration of the volcanic structure shows considerable detail. The E-W density cross-section (Figure 13) shows a vertical channel of 4 km width, extending vertically to 5 km, containing three density minima at elevations of +1200 (A), +2500 (B) and +3500 m (C), located under the summit, realizing a succession of magma deposits instead of a single chamber in this volcano.

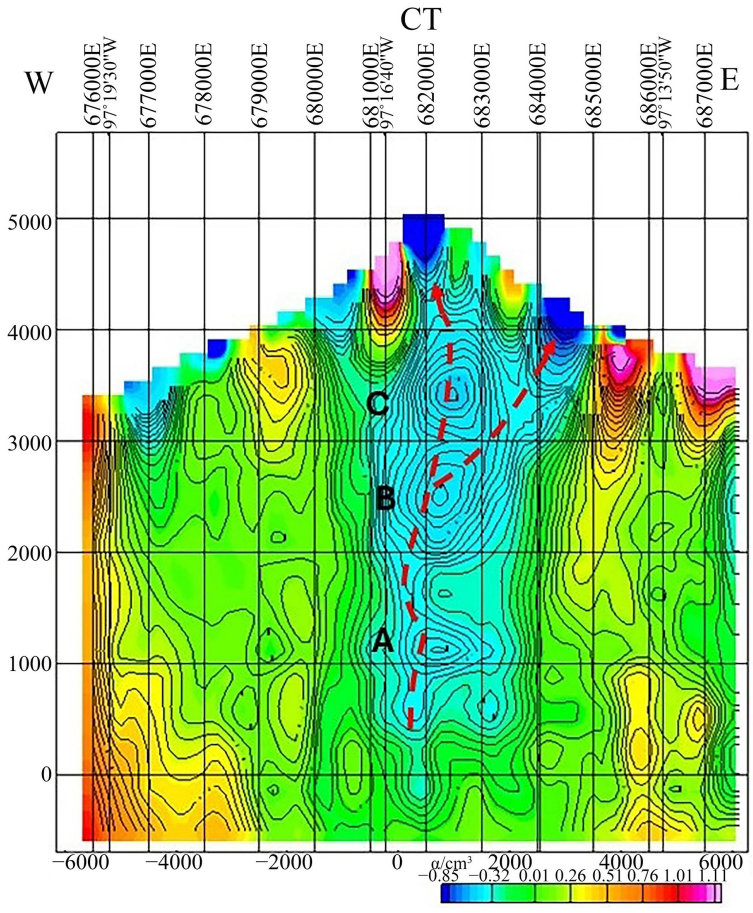


Figure 13. E-W cross-section through the summit of CT at 250 m resolution (Line E, Figure 9). Three low-density minima are centered at elevations of (A) +1200, (B) +2500, and (C) +3500 m. The density minima channel extends horizontally from −2000 to +2000 m. A bifurcation to the E of the feeding channel starts at +2500 masl, ending at a surficial, low-density concentration. The color scale represents density values +2.67g/cm³.

This result supports the proposal that the magma chamber of CT is stratified [7], based on the observation of the increment in dacitic Plinian eruptions, which occurred four times in the Holocene related to the increased volumes of dacitic magma beneath CT. The proponents also indicate that it is probable that magma is accumulating at the interface between the shear faults and the superficial SW-NE extensional faults, where the regime goes from compressional to extensional. However, they do not find it clear if the surface volcanic alignment reflects several individual magma reservoirs or the shape of a single reservoir under the whole volcanic complex.

At the lower resolutions analyzed previously, this region appeared as an elongated, vertical density minimum. Two dashed lines indicate probable trajectories for the distribution of magmatic materials within the volcanic cone, one ends at the chimney, and the other terminates on the surface of the E-side of the volcanic structure. The concentration of the low-density material on the surface of the E-side of the volcano intuitively appears as a region with a high probability of explosive activity, since volatiles normally accompany the magmatic materials, which tend to be more easily released on, or close to the surface. Additional geophysical determinations of this region of the volcano could be seismic and ground deformation data. Low-density concentrations on the W flank do not appear as directly fed by the magmatic chambers.

The configuration of the magmatic deposits along the N-S density cross-section (**Figure 14**) differs somewhat from that found in the E-W cross-section. Notwithstanding, the elevations of the three density minima are like those detected previously. Along this orientation, the volcano's summit is covered with high-density materials, probably representing layers of erupted lava flows or domes intruded in those locations. From this perspective, the chimney shows a low-density vertical region at the summit but no direct connection with the magma chamber is observed. In this projection the surficial, low-density region located at 210,3000 N also appears in **Figure 12** and **Figure 15**.

A horseshoe-shape escarpment on the upper, N side of the edifice that they interpreted as an amphitheater-like valley formed by glacial erosion, or a glacial cirque [2]. In **Figure 14** we combine the N-S density cross-section with the corresponding topographic profile, where the escarpment is shown to coincide with the boundary between low- and high-density regions. The low-density region corresponds to a conduit directly connected with the main plumbing system of the volcano, and the high-density region under it probably corresponds to an intrusion. The combined effect of magmatic products accompanied by volatiles, and the intrusion emplacement could have induced the debris avalanche that traveled 12 km to the W, from the summit: the avalanche reportedly being older than 38 ka [6] [25].

**NW-SE cross-section at 250-m**

In this paragraph we add geophysical arguments to the reconstruction of the Ancestral Teteltzingo. The density cross-section in **Figure 15** goes through the summits of SN and CT and it is flanked by high-density regions; its central part shows the lowest density values between Lines 2 and 3 (**Figure 15**). To the SW,

Sierra Negra is the first volcanic edifice in the density cross-section; it is considered an extinct volcano since it has had no activity in the Holocene. However, in Figure 16, SN displays a low-density area bordering the high-density region; the presence of abundant low-density materials at the summit of SN tends to contradict the statement that this is an extinct volcano, considering that the density distributions at SN and CT are quite similar, and the latter being an active volcano. For this reason, in the next section we include specific observations on SN.

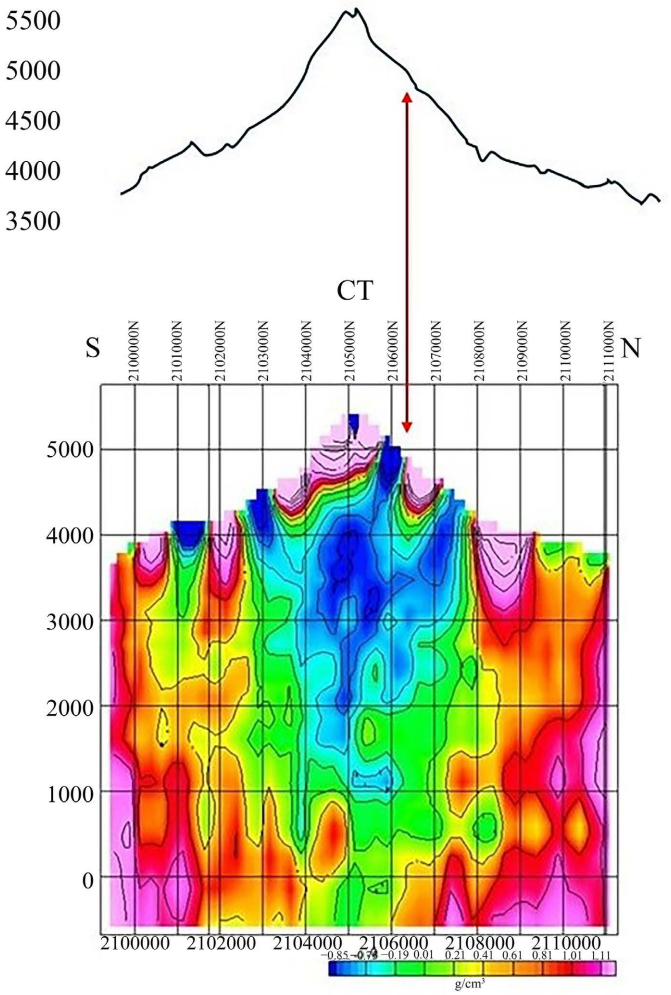


Figure 14. Density cross-section along the (N-S) magenta line within the smallest rectangle in the map of Figure 2. The extent is 12 km, and the resolution is 250 m; the model reaches a depth of −500 m. CT's topographic profile is now clearly delineated; it shows an extended region of high-density materials close to the summit, and three low-density conduits reach the surface. The topographic profile is at the same horizontal scale as the cross-section, partly justifying the presence of high-density regions at the summit. We infer that there are other domes, not exposed to the surface, that yield the observed high-density distribution around the summit of CT. Immediately SW of the summit, there is a low-density region that appears to be a new discharge trajectory (red line). Showing a notch in the N slope; a vertical arrow shows the correspondence with the boundary of low- and high-density regions. The color scale represents density values +2.67 g/cm$^3$.

Sierra Negra has an age of 290 ka [1] (see Table 1), coinciding in time with the collapse of the ATE. Figure 15 shows that between Lines 1 and 4, there is a medium- to low-density region flanked by high-density formations, underlying SN, CT, and CDC.

Although the existence of high-density materials on or close to the summit of a volcano is not a rare occurrence, the abundant high-density materials in the summit of CT largely exceed the norm, requiring an explanation. We offer a tentative one: the collapse of the summit at 13 ka created a large crater 4 - 5 km wide [3], in which a new cone grew, corresponding to the region between Lines 2 and 3 in Figure 15. We have reported the occurrence of high-density materials near volcanic summits in various publications (e.g., Popocatépetl's El Ventorrillo [22], associated with blockage of the active chimney. A large dome on the E side of the summit of CT was reported [7], which would be registered here as a high-density anomaly.

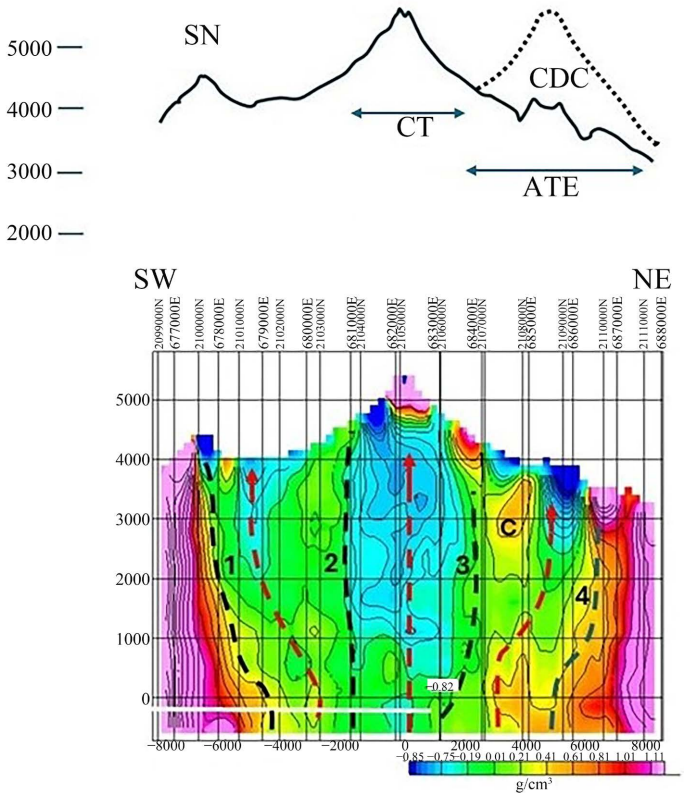


Figure 15. SW-NE density cross-section (Line C in Figure 9) obtained from the 3D gravity inversion, at 250 m resolution, and the corresponding topographic profile (from GeomapApp) along the summits of Sierra Negra (SN), Citlaltépetl (CT), and the Chichimeco Dome Complex (CDC). The dashed line in the topographic profile represents the possible location and size of the ATE. Black lines indicate limits within the density cross-section, and red lines show possible trajectories for volcanic materials flowing to the surface. Lines 1 - 2 limit a mid-density region between SN and CT. Lines 2 - 3 delimit a central, low-density region, and Lines 3 - 4 contain low-, mid-, and high-density regions. C, collapsed region. The color scale represents density values +2.67 g/cm$^3$.

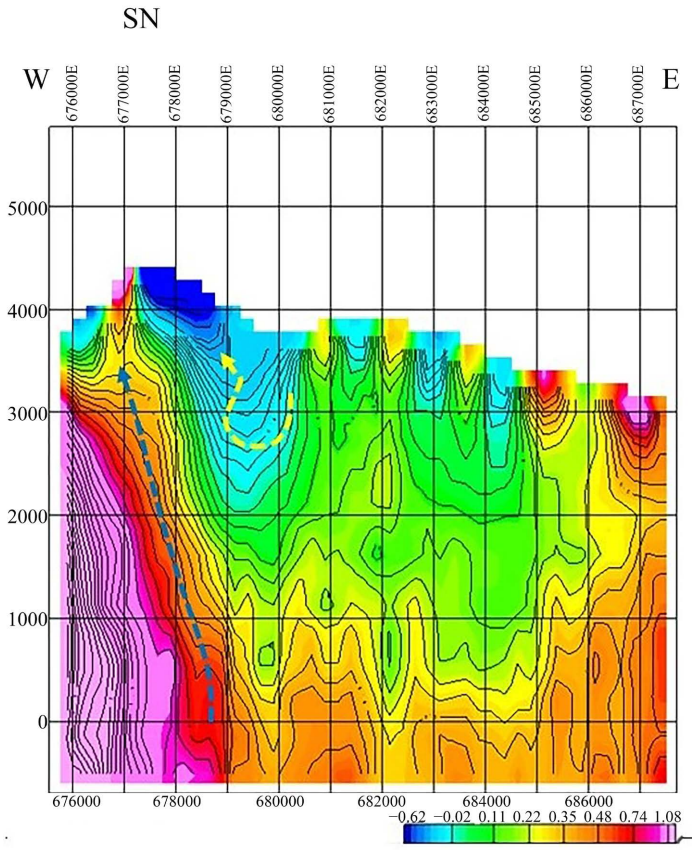


**Figure 16.** Density cross-section in the E-W direction (Line A, in **Figure 9**) through the summit of Sierra Negra (SN) at 250 m resolution. The objective is to show a complementary view of the summit of SN. The summit appears shared by a high- and a low-density region; the continuation downwards of the high-density regions suggests that this was a chimney of the original structure that became occluded/abandoned. The dashed lines show two possible trajectories: the dark one corresponds to an old trajectory that appears now replaced by the yellow one; its trajectory indicates lateral feeding. The color scale represents density values +2.67 g/cm$^3$.

The Chichimeco Dome Complex is described as a group of domes dispersed within an ellipse [3], accompanied by aerial deposits that they attribute to emissions of lateral conduits associated with the dome extrusions, rather than emissions from the central crater. The date of extrusion of the CDC has been placed between 17 and 12.9 ka [7]; the dome complex has a volume of 8 km$^3$ extruded in ~4000 years. Thus, dome extrusion occurred quite close in time to the collapse of the summit at 13 ka, and we attribute it to resurgent activity of the ATE. In **Figure 15**, between Lines 3 and 4, high-density materials (C) are observed; we note that this type of material is exclusively identified within this section. Given its size and position, we attribute it to the material of the collapsed cone of ATE. Next to it, to the NE, there is a low-density region that coincides with the CDC.

## 4. Sierra Negra

Volcanism at Citlaltépetl is aligned along a SW-NE tectonic lineament that is a

superficial tectonic system generated by a buried E-W sinistral shear fault [26] Sierra Negra is located SW of CT (**Figure 1**); it has been called a parasitic volcano to Citlaltépetl [27] [28]; however, evidence is mounting that this structure is an independent volcano, whose age has been placed at 290 ka [1].

Although SN has been considered inactive, it has been pointed out that some fluxes and pyroclastic deposits of this volcano appear, morphologically, quite recent, suggesting it has been active in recent times [3]. A ballistic bomb on the summit of SN was reported in a well-preserved impact crater [7]. The crater rims are made of loose sand, indicating that the impact could be quite young, possibly from this century. In addition, the tephra of Ciudad Serdán is attributed by those authors to Sierra Negra, and their ages do not exceed a few tens of thousands of years.

The N-S cross-section in **Figure 17** defines a mid- to low-density region above +1000 m, which appears to be, or had been, fed through four channels between -500 and +1000 m elevations. The existence of a collapsed region (caldera?) immediately N of the summit of SN, with what we interpret as a shallow magma/volatiles deposit centered at +3500 m, may be a region of recent reactivation, justifying the surficial activity described above.

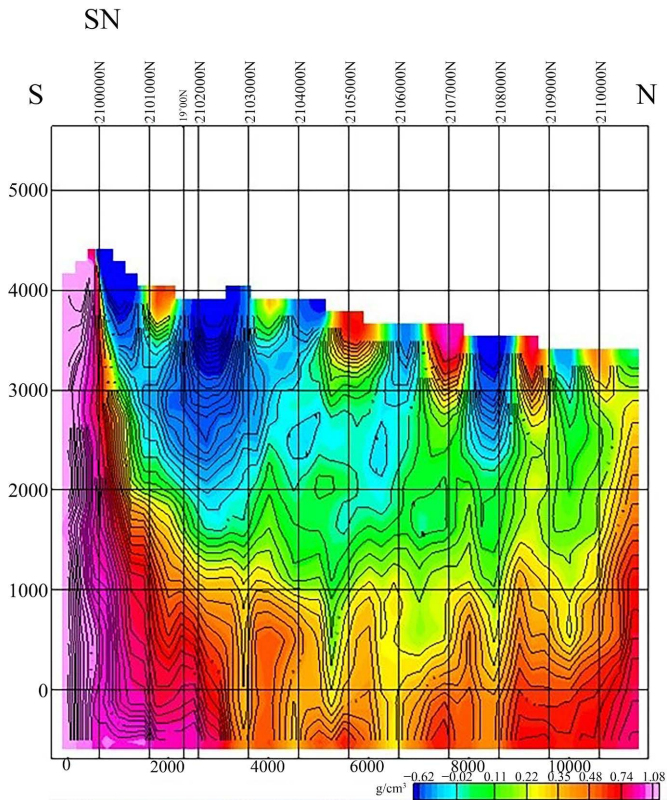


**Figure 17.** Density cross-section in the N-S direction (Line B, in **Figure 9**) through the summit of Sierra Negra (SN) at 250 m resolution. The summit of SN contains equal amounts of high- and low-density materials; 2 km to the N, a small caldera-type formation is underlaid by an important low-density concentration extending down to +2500 m, which we interpret as the feeding source of the low-density portion of SN. Between +1000 and −500 m elevation, four feeding channels can be clearly identified. The color scale represents density values +2.67 g/cm$^3$.

## 5. Discussion

The alignment along the SW-NE direction of three volcanic structures: SN, CT, and CDC, and the associated low-density region under them, as well as the orientation of the associated Bouguer anomaly, suggest that a cortical fault in that direction is the path of the volcanic materials building those structures. Another major volcanic alignment occurs northward, extending from CT to Las Cumbres Volcanic Field, ending at Nauhcampatépetl (Cofre de Perote, 4282 m), an extinct volcano. Based on the observed remains of fault scarps left by the collapse at 33 ka [7] and constrained by the Bouguer anomaly associated with the CT (**Figure 7**), we proposed the existence of the ATE volcano (**Figure 16**). Under the proposed location of the ATE volcano, we found a high-density region, which we attribute to the collapse of the ATE cone, probably building a caldera.

As documented in several Mexican volcanoes, blocking the chimney often destroys their summits. Nevado de Toluca has been active over the past 2.6 My, emitting andesitic lava flows and pyroclastic deposits, and the latest activity was recorded at 3.3 ka. Explosive eruptions were identified, and flank collapses severely modified the volcano's original morphology [29]. The original edifice of Nevado de Toluca has been destroyed twice, as indicated by debris avalanches, lahars, and fluvial deposits observed on its south flank [30] [31]. Nevado de Toluca has a peculiar plumbing system, with two branches that surround, but do not completely enclose, the upper portions of the structure, conveying magmatic products to the volcano's summit, reminding the structural characteristics reported here for Citlaltépetl Volcano [13].

Nevado de Colima caldera collapses were reported [32], registering at least three major collapses of this volcano during its active period; the three different calderas that resulted from the collapses were mapped [4]. The ancestral Colima Fuego Volcano also experienced a collapse [10]; a new volcanic cone is being built upon the collapsed structure.

Popocatépetl Volcano, located along the Sierra Nevada, has an ancestral edifice named El Ventorrillo Volcano [33] that at 14.1 ka gave rise to the present edifice of Popocatépetl, where we also found a high-density region blocking what was the original chimney, deflecting activity toward the E [22].

In **Figure 13**, we observe that a high-density region appears to partially block the chimney on its W side. And in **Figure 14**, it is observed that three low-density conduits appear to circumvent the high-density regions close to the summit. The inference can be made that above +4000 m, high-density materials have been accumulating on the edifice of CT, blocking direct paths to the chimney. The present concurrence in CT of high-density materials around the summit, partial blocking of the chimney, and deviation of low-density channels from the magma chambers to the slopes of the volcano prefigures a risky scenario.

## 6. Conclusions

Starting from the reported fault scarp positions of the collapse of Tetelzingo crater

at 32 ka, and using the Bouguer anomaly as a constraint, we completed a version of the continuous rim of the collapse. The shape of the reconstructed rim suggested the presence of two neighboring volcanoes: CT and ATE. In the collapsed portion of CT, a new cone grew, whilst the Tetelzingo structure was obliterated by pyroclastic ejecta and lava flows. Dome extrusion occupied the central portion of the ATE at <8 ka as a resurgent activity. Density distributions associated with this region support the existence of a volcano at the inferred ATE location.

The existence of a stratified magma chamber was proposed based on geologic arguments [7] [34] without specifying the characteristics of the stratification. We found a stack of three low-density regions under the chimney of CT that fulfill the stratification criterion and allow size determination, which will allow future modeling of magma/volatiles injection into the system.

An anomalous distribution of high-density materials at the summit of CT was found. Other volcanic structures show high-density materials near the summit, but are less prominent. We attribute their existence in CT to dome extrusions and high-density fluxes close to the summit area, some of which have been mapped by several authors. Clearly, these heavy materials on the summit represent hazard risks due to potential instability, and their location and distribution should be the subject of future studies.

Sierra Negra volcano has often been described as an extinct volcano, despite previous observations that suggest recent activity. Not being the central objective of this study, we only obtained three density cross-sections through this structure. All of them show low-density materials at the summit and in some surrounding areas, like those observed at CT. We suggest that reactivation activity may be responsible for the accumulation of these low-density materials. Additional studies should be carried out on this volcano to determine its actual state.

## Acknowledgements

This study has been supported by IIMAS and the Geophysics Institute, both at UNAM; we acknowledge material support from both institutions. This research did not receive any specific grant from funding agencies in the public, commercial, or nonprofit sectors.

## Conflicts of Interest

The authors declare no conflicts of interest regarding the publication of this paper.

## References

[1] Carrasco-Nuñez, G. (2000) Structure and Proximal Stratigraphy of Citlaltepetl Volcano (pico De Orizaba), Mexico. In: *Cenozoic Tectonics and Volcanism of Mexico*, Geological Society of America, 334. https://doi.org/10.1130/0-8137-2334-5.247.

[2] Siebe, C., Abrams, M. and Sheridan, M.F. (1993) Major Holocene Block-and-Ash Fan at the Western Slope of Ice-Capped Pico De Orizaba Volcano, México: Implications for Future Hazards. *Journal of Volcanology and Geothermal Research*, **59**, 1-33. https://doi.org/10.1016/0377-0273(93)90075-3

[3] Robin, C. and Cantagrel, J.M. (1982) Le Pico de Orizaba (Mexique): Structure et evolution d'un grand volcan andesitique complexe. *Bulletin Volcanologique*, **45**, 299-315. https://doi.org/10.1007/bf02597254

[4] Robin, C., Komorowski, J., Boudal, C. and Mossand, P. (1990) Mixed-Magma Pyroclastic Surge Deposits Associated with Debris Avalanche Deposits at Colima Volcanoes, Mexico. *Bulletin of Volcanology*, **52**, 391-403. https://doi.org/10.1007/bf00302051

[5] Sheridan, M.F., Siebe, C., Kahle, A. and Abrams, M. (1990) Remotely Sensed Data for Volcanoes of the Trans-Mexican Volcanic Belt. *The Tectonics, Geophysics, and Volcanism of Mexico: A Symposium*, New Orleans, 12-14 April 1990, 102.

[6] Hoskuldsson, A., Robin, C. and Cantagrel, J.M., (1990) Repetitive Debris Avalanche Events at Volcano Pico de Orizaba, Mexico and Their Implications for Future Hazard Zones. 1990 *IAVCEI International Volcanological Congress*, Mainz, 3-8 September 1990, 75.

[7] Hoskuldsson, A. and Robin, C. (1993) Late Pleistocene to Holocene Eruptive Activity of Pico De Orizaba, Eastern Mexico. *Bulletin of Volcanology*, **55**, 571-587. https://doi.org/10.1007/bf00301810

[8] Ryan, W.B.F., Carbotte, S.M., Coplan, J.O., O'Hara, S., Melkonian, A., Arko, R., *et al.* (2009) Global Multi-Resolution Topography Synthesis. *Geochemistry, Geophysics, Geosystems*, **10**, 1-9. https://doi.org/10.1029/2008gc002332

[9] Hirt, C., Claessens, S., Fecher, T., Kuhn, M., Pail, R. and Rexer, M. (2013) New Ultrahigh-Resolution Picture of Earth's Gravity Field. *Geophysical Research Letters*, **40**, 4279-4283. https://doi.org/10.1002/grl.50838

[10] Alvarez, R. and Yutsis, V. (2015) Southward Migration of Magmatic Activity in the Colima Volcanic Complex, Mexico: An Ongoing Process. *International Journal of Geosciences*, **6**, 1077-1099. https://doi.org/10.4236/ijg.2015.69085

[11] Guevara-Betancourt, R., Yutsis, V., Varley, N., Almaguer, J., Alvarez, R., Calderón-Moctezuma, A., *et al.* (2023) Insights into the Plumbing System of Colima Volcanic Complex. *Journal of Volcanology and Geothermal Research*, **433**, Article 107711. https://doi.org/10.1016/j.jvolgeores.2022.107711

[12] Alvarez, R. and Camacho, M. (2023) Plumbing System of Hunga Tonga Hunga Ha'apai Volcano. *Journal of Earth Science*, **34**, 706-716. https://doi.org/10.1007/s12583-022-1792-0

[13] Alvarez, R. and Camacho, M. (2023) Applying High-Resolution Gravity Analysis to Volcanic Plumbing Systems: The Case of Nevado de Toluca volcano, Mexico. *Transactions on Engineering and Computing Sciences*, **11**, 184-207.

[14] Alvarez, R., Camacho, M. and Rivera-Calderón, E. (2024) The Internal Structure of Paricutin and Tancítaro Volcanos, Mexico, From Rock Density Distributions. *Transactions on Engineering and Computing Sciences*, **12**, 50-69.

[15] Hildenbrand, T.G., Briesacher, A., Flanagan, G., *et al.* (2002) Rationale and Operational Plan to Upgrade the US Gravity Database. USGS Open File Report. Geology, Minerals, Energy and Geophysics Science Center.

[16] Weatherall, P., Tozer, B., Arndt, J.E., *et al.* (2021) The GEBCO_2021 Grid a Continuous Terrain Model of the Global Oceans and Land. https://www.bodc.ac.uk/data/published_data_library/catalogue/10.5285/c6612cbe-50b3-0cff-e053-6c86abc09f8f

[17] NOAA (2022) National Centers for Environmental Information: ETOPO 2022 15 Arc-Second Global Relief Model. NOAA National Centers for Environmental Information.

[18] Kane, M.F. (1962) A Comprehensive System of Terrain Corrections Using a Digital Computer. *Geophysics*, **27**, 455-462. https://doi.org/10.1190/1.1439044

[19] Nagy, D. (1966) The Gravitational Attraction of a Right Rectangular Prism. *Geophysics*, **31**, 362-371. https://doi.org/10.1190/1.1439779

[20] Suryanata, P.B., Bijaksana, S., Dahrin, D., Nugraha, A.D., Harlianti, U., Putra, P.R.A., *et al.* (2024) Subsurface Structure of Bali Island Inferred from Magnetic and Gravity Modeling: New Insights into Volcanic Activity and Migration of Volcanic Centers. *International Journal of Earth Sciences*, **113**, 523-538. https://doi.org/10.1007/s00531-024-02398-7

[21] Alvarez, R. and Yutsis, V.V. (2017) Potential Fields Modeling of the Serdán Oriental Basin, Eastern Mexico. *Journal of South American Earth Sciences*, **80**, 375-388. https://doi.org/10.1016/j.jsames.2017.10.003

[22] Alvarez, R. and Camacho-Ascanio, M. (2025) Gravimetric Definition of the Magmatic Chambers of the Popocatépetl-Iztaccíhuatl Volcanic Complex, Mexico. *Earth Science and Engineering*, 4, 1-18. https://doi.org/10.57237/j.earth.2025.01.001

[23] Rodríguez-Elizarrarás, S., Komorowski, J.-C. and Abrams, M. (1994) The Quetzalapa pumice at Las Cumbres complex: Product of a powerful Plinian eruption in the eastern Trans Mexican Vocanic Belt. 1994 *International Volcanological Congress*, Ankara, 12-16 September, Abstracts p. 81.

[24] Siebe, C., Macías, J.L., Abrams, M., Rodríguez, S., Castro, R. and Delgado, H. (1995) Quaternary Explosive Volcanism and Pyroclastic Deposits in East, Central Mexico: Implications for Future Hazards. In: *Guidebook for the* 1995 *Annual Meeting of the Geological Society of America*, Basin Research Institute, Center for Coastal, Energy & Environmental Resources, Louisiana State University, 1-47.

[25] Cantagrel, J.M. and Robin, C. (1979) K-Ar Dating on Eastern Mexican Volcanic Rocks—Relations between the Andesitic and the Alkaline Provinces. *Journal of Volcanology and Geothermal Research*, **5**, 99-114. https://doi.org/10.1016/0377-0273(79)90035-0

[26] Hoskuldsson, A. (1992) Les debris-avalanches du Pico de Orizaba (Mexique). *Bulletin de la Société géologique de France*, **19**, 5-7.

[27] Robin, C. (1981) Relations Volcanologie-Magmatologie-Geodynamique: Application au passage entre volcanism alcalin et andesitique dans le sud Mexicain (Axe transmexicain et provence alcaline oriental). These Doctorat d'etat Universite Clermont-Ferrand II.

[28] Negendank, J.F.W., Emmermann, R., Krawczyk, R., Mooser, F., Tobschall, H. and Werle, D.J. (1985) Geological and Geochemical Investigations on the Eastern Trans-Mexican Volcanic Belt. *Geofísica Internacional*, **24**, 477-575. https://doi.org/10.22201/igeof.00167169p.1985.24.4.2178

[29] Torres-Orozco, R., Arce, J.L., Layer, P.W. and Benowitz, J.A. (2017) The Quaternary History of Effusive Volcanism of the Nevado De Toluca Area, Central Mexico. *Journal of South American Earth Sciences*, **79**, 12-39. https://doi.org/10.1016/j.jsames.2017.07.008

[30] Macías, J.L., García-Palomo, A., Arce, J.L., Siebe, C., *et al.* (1997) Late Pleistocene—Holocene Cataclysmic Eruptions at Nevado de Toluca and Jocotitlán Volcanoes, Central Mexico. In: Kowallis, B.J., Ed., *Proterozoic to Recent Stratigraphy, Tectonic and Volcanology, Utah, Nevada, Southern Idaho and Central Mexico*, Brigham Young University, 493-528.

[31] Capra, L. and Macías, J.L. (2000) Pleistocene Cohesive Debris Flows at Nevado de To-

luca Volcano, Central Mexico. *Journal of Volcanology and Geothermal Research*, **102**, 149-167. https://doi.org/10.1016/s0377-0273(00)00186-4

[32] Robin, C., Mossand, P., Camus, G., Cantagrel, J., Gourgaud, A. and Vincent, P.M. (1987) Eruptive History of the Colima Volcanic Complex (Mexico). *Journal of Volcanology and Geothermal Research*, **31**, 99-113. https://doi.org/10.1016/0377-0273(87)90008-4

[33] Sosa-Ceballos, G., Macías, J.L., García-Tenorio, F., Layer, P., Schaaf, P., Solís Pichardo, G., *et al.* (2015) El Ventorrillo, a Paleostructure of Popocatépetl Volcano: Insights from Geochronology and Geochemistry. *Bulletin of Volcanology*, **77**, Article No. 91. https://doi.org/10.1007/s00445-015-0975-2

[34] Hildreth, W. (1981) Gradients in Silicic Magma Chambers: Implications for Lithospheric Magmatism. *Journal of Geophysical Research*: *Solid Earth*, **86**, 10153-10192. https://doi.org/10.1029/jb086ib11p10153